Journal of Translational Medicine

RESEARCH

Open Access

Comparison of functional characterization of cancer stem cells in different tumor tissues of pseudomyxoma peritonei

Haipeng Zhou[1], Hongbin Xu[1], Shaojun Pang[1], Lubiao An[1], Guanjun Shi[1], Chong Wang[1], Pu Zhang[1], Xiwen Fan[1], Jing Yang[2], Shiyi Tang[2], Yiyan Lu[3], Lifei Yu[1], Feng Chen[1] and Ruiqing Ma[1*]

Abstract

Background Pseudomyxoma peritonei (PMP) is a rare malignant peritoneal tumor that readily recurs and metastasizes. Studies have shown that cancer stem cells (CSCs) play an important role in tumor recurrence, metastasis, and prognosis.

Objective In this study, our aim was to isolate CSCs from various tissues of PMP patients and compare their proliferation, migration, and anti-inflammatory abilities.

Methods We identified CSCs subsets with markers $CD133^+$, $CD166^+$, and $CD133^+/CD166^+$ at the gene level using single-cell mRNA sequencing (scRNA-seq). Appendiceal CSCs (AC), peritoneal CSCs (PC), and mucous CSCs (MC) were obtained using MACSQuant Tyto sorting technology and FlowSight imaging flow cytometry. The cells were cultured and markers were identified. Finally, the functional phenotypes of the three cell types were compared.

Results CSCs content was highest in the appendiceal tumor tissue and lowest in the mucous tissue. The cell viability rate of the sorted CSCs was above 98%, and the positive rate of $CD133^+$ and $CD166^+$ was 70–80%, and $CD133^+/CD166^+$ was about 30%. Among the three types of CSCs, MC had the highest proliferation ability, and TNF-α has the greatest inhibitory effect on AC migration.

Conclusion AC in patients was more inert and anti-inflammatory, whereas abdominal cavity MC and PC were more active. This study revealed the biological characteristics of CSCs in different tumor tissues of patients with PMP, providing a reference for future targeted CSCs therapy.

Keywords Pseudomyxoma peritonei, Cancer stem cells, Single-cell RNA sequencing, Cell sorting, Cell function

*Correspondence:
Ruiqing Ma
maruiqing2014@126.com
[1]Department of Myxoma, Aerospace Center Hospital, Beijing 100049, China
[2]Space Medical Center, Aerospace Center Hospital, Beijing 100049, China
[3]Department of Pathology, Aerospace Center Hospital, Beijing 100049, China

Background

Pseudomyxoma peritonei (PMP) is an extremely rare peritoneal tumor that is estimated to affect 1–3 people per million per year [1]. PMP tumor cells mainly originate from the appendix (94%) [2] followed by the ovary [3]. The onset of PMP is insidious, mostly due to rupture of an appendiceal mucocele. Tumor cells with the ability to secrete mucin are implanted in the peritoneum, omentum, and surface of abdominal organs. They secrete a large amount of jelly-like mucus into the abdominal cavity, occupying the effective space of the abdominal cavity, leading to progressive abdominal distension, abdominal pain, intestinal obstruction, and eventually death. In addition, because the pathogenic cells are wrapped in mucus, they can exhibit high drug resistance, and it is difficult to completely remove them surgically, which ultimately causes disease relapse [4, 5] (Fig. 1).

Currently, recognized strategies for the treatment of PMP include cytoreductive surgery (CRS) and hyperthermic intraperitoneal chemotherapy (HIPEC) [6, 7]. Studies from different centers have shown that after standard CRS+HIPEC treatment, the lowest rate of disease recurrence is 18.6%, generally between 26.4% and 46%, and the 5-year and 10-year survival rates are 71% and 42%, respectively [8]. CRS+HIPEC has relatively good survival benefits, but still cannot prevent disease recurrence and metastasis. Moreover, PMP often responds poorly to systemic chemotherapy, and there are no other effective treatments for patients who cannot be treated with CRS+HIPEC [9]. Therefore, finding a new strategy for the treatment of PMP based on CRS+HIPEC is an urgent problem.

Cancer stem cells (CSCs) are a small subset of undifferentiated cells present in tumor tissues that have the potential for self-renewal and strong tumorigenic potential [10]. CSCs were first found in hematological malignancies and then in colorectal, liver, head and neck, brain, pancreatic, breast, and ovarian tumors [11–15]. CD133 [16] and CD166 [17] are currently used as markers of tumor stem cells. Hermann et al. [18] found that CSCs expressing CD133 in adenocarcinoma tissues were highly resistant to standard chemotherapy. Gulam et al. [19] used CD133 and CD166 as markers of lung cancer stem cells and found that $CD166^+$ cells were relatively resistant to apoptosis. Kim et al. [20] used pyrivine to act on $CD133^+/CD166^+$ stem cell populations, inhibiting the progression of metaplasia in mice and promoting the recovery of normal oxyntic glands. Leila et al. [21] showed that the high expression of $CD166^+$ tumor stem cells in gastric cancer was directly correlated with lymphatic and subserous invasion. The mechanisms by which CSCs cause tumor recurrence and metastasis differ between tumors. Therefore, it is necessary to fully understand the biological characteristics of CSCs in PMP.

We can observe that the appendiceal tumor tissue, mucous tissue, and peritoneal tumor tissue of PMP patients exhibit three distinct lesions with different appearances. Therefore, we hypothesize that the biological characteristics of cancer stem cells in these three tissues would vary. Thus, this study aims to conduct a comparative analysis of the biological characteristics of appendiceal CSCs (AC), peritoneal CSCs (PC), and mucous CSCs (MC) derived from PMP patients.

Methods

Patient and tissue selection

Patients with appendiceal PMP were randomly selected prior to surgery ($N=6$). The enrolled patients were newly diagnosed with no history of other tumors. None of the patients had received chemotherapy, targeted therapy, or immunotherapy before surgery. If postoperative pathology reports ruled out appendiceal PMP, the patient was invited to withdraw from the study. Appendiceal tumor, mucous tissue, and peritoneal tumor tissues were chosen as the experimental specimens. All human tissues were handled in accordance with protocols approved by the hospital's Ethics Committee (Application No. 2024-024).

Preparation of single cell suspensions from different tumor tissues

Appendiceal tumor tissue, mucous tissue, and peritoneal tumor tissue were preserved in a tissue preservation

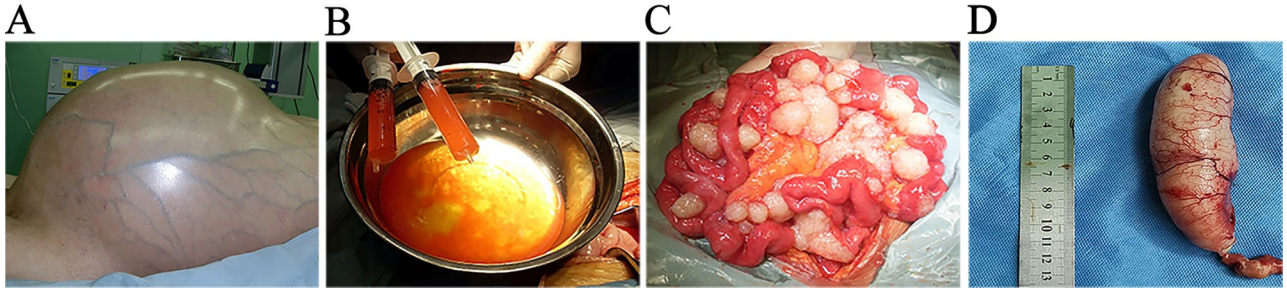

Fig. 1 Clinical features of PMP. **A**. A large amount of mucus in the abdominal cavity leads to severe intestinal obstruction and frog-like abdomen. **B**. The "jelly"-like mucus in the abdominal cavity was removed during the operation. **C**. Tumor cells were widely planted on the omentum and peritoneum. **D**. A large appendix full of mucus

solution (130-100-008, Miltenyi). Tumors generally had a volume not exceeding 1.0 cm^3 and a mass ranging between 0.6 and 0.8 g. The tissues were carefully dissected and transferred to sterile 50 mL eppendorf tubes. Subsequently, 5 mL of our self-developed tissue lysate was added to each tube for digestion at 80 rpm and 37 ℃ on a shaking table for a duration of 1–3 h. Once the digestion process was complete, the supernatant was collected by centrifugation at 50 g for 10 min to obtain a single-cell suspension.

Single-cell mRNA sequencing of CSCs

CSC subpopulations were identified using single-cell mRNA sequencing (scRNA-seq). A cell suspension containing 1×10^6 cells was rapidly loaded into a 3' chemical chromium microfluidic chip, followed by reverse transcription of the RNA from these cells. Sequencing libraries were constructed using reagents from the Chromium single-cell 3' v2 kit (10× Genomics, Pleasanton, California) as per the manufacturer's instructions. Illumina sequencing was performed according to the manufacturer's instructions (Illumina, San Diego, California). Intestinal cell type markers were determined based on The Caner Genome Atlas (TCGA) and Gene Expression Omnibus (GEO) databases (Table S1), and cells were annotated as epithelial cells, endothelial cells, fibroblasts, mast cells, smooth muscle cells, adipocytes, gonorrhea lymphocytes and myeloid lymphocytes. Based on previously reported mutated genes in PMP, along with colorectal cancer and appendix cancer markers in TCGA and GEO databases, the epithelial cell population was further annotated as PMP tumor cells and normal epithelial cells (Table S2). Subsequently, $CD133^+$, $CD166^+$ and $CD133^+/CD166^+$ markers were used to screen for CSCs subsets within the selected PMP tumor cell population.

Flow cytometry and cell sorting of CSCs

Cells were incubated with antibodies for the cell markers CD133 and CD166. The cells were then digested, washed once with buffer (pH 7.2 phosphate buffered saline (PBS), 0.5% bovine serum albumin), and centrifuged at 500 × g for 5 min at 4 °C. Fc receptors were blocked using normal mouse serum for 10 min at 25 °C. Subsequently, the cells were surface-stained with CD133-PE (12-1338-42; Thermo Fisher Scientific, Waltham, Massachusetts, USA) and mouse anti-human antibody (Cat. #562799, BD Biosciences, Franklin Lake, New Jersey, USA), CD166-BV421 (404044182, Thermo Fisher Scientific, Waltham, Massachusetts, USA) and mouse anti-human antibody (Cat. #FAB2585A, R&D Systems, Minneapolis, MN, USA), or CD166-APC (17-1661-82, Thermo Fisher Scientific, Waltham, Massachusetts, USA) and mouse anti-human antibody (Cat. #130-093-581, Miltenyi Biotec, Bergisch-Gladbach, Germany) for a duration of 30 min at 4 °C. After surface staining, the CSCs underwent another wash step using the aforementioned buffer followed by centrifugation at 500 × g for 5 min at 4 °C. The resulting cell pellet was resuspended in the same buffer for flow cytometry and cell sorting.

MACSQuant Tyto cell sorting

The cells incubated with antibodies for cell sorting were transferred to a MACSQuant Tyto Cartridge. The input sample contained 4×10^6 CSCs in 10 mL of MACSQuant Tyto Running Buffer. Logical gating hierarchies were constructed using the MACSQuant Tyto software prior to sorting. Cell debris, doublets, and dead cells were excluded by gating, and a gate was set on the target cells. The samples were sorted at a flow rate of 5 mL/h and a pressure of approximately 150 mbar. After sorting, the negative cells were analyzed using a FlowSight imaging flow cytometer to assess cell purity and yield. CD133 and CD166 expression was detected using a FlowSight imaging flow cytometer, and simultaneously approximately 4000–5000 cells were selected and visualized. Based on their morphology, size, and positivity rate, the sorting strategy was adjusted in real time to ensure that the positivity rate of target cells reached more than 90 ~ 95% while maintaining cell viability above 95%.

FlowSight image flow cytometric analysis

Cells were acquired using a FlowSight imaging flow cytometer (Amnis, part of EMD Millipore, Massachusetts, USA), and cell debris and dead cells were identified and removed based on the aspect ratio and area of the cells. Each analysis yielded approximately 5000 cells, with BV421 detected in Channel 11 and PE acquired in Channel 3. Single colour control samples were compensated using a .rif compensation matrix before being converted to data analysis files (.daf) and compensated image files (.cif) with identical settings. The Ideas software version 6.2 was used for data analysis.

Cultivation and identification of CSCs

The cells were cultured in a customized medium at 37 °C within a humidified incubator containing 5% CO_2 gas mixture (Text S1). The identification of CSCs was accomplished through the utilization of immunofluorescence staining as well as flow cytometry techniques. To identify the CSC population by immunofluorescence staining, a polyclonal rabbit anti-CD133 antibody (1:200, Cat. #SAB5701045, Sigma-Aldrich, St. Louis, Missouri, USA) and polyclonal mouse anti-CD166 antibody (1:50, Cat. #AF1172, R&D Systems, Minneapolis, Minnesota, USA), were employed. Cell nuclei were counterstained with 4′6-diamidino-2-phenylindole (DAPI) (1:20, Cat. #5748, R&D Systems) for five minutes before observation under

a fluorescence microscope (IX-70; Olympus Corporation, Tokyo, Japan).

Cell proliferation assays

The cell proliferation was assessed using the Cell Counting Kit-8 (CCK-8) assay (Cat. #PA1-36074, Thermo Fisher Scientific, Waltham, Massachusetts, USA). Three types of CSCs were seeded at a density of 5000 cells per well in a 96-well plate. The outermost circle of the plate contained volatile liquid and was supplemented with PBS for moisturizing purposes only. The cells were cultured at 37 °C and 5% CO_2 for 24 h. In the blank control group, an equal volume of medium without any cells was added to each well as a negative control. Six replicate wells were set up for each experimental group without adding any cells. At different time points (days 1, 3, 5, 7, 9, and 11), a solution containing CCK-8 reagent (10μL) was added to each well and incubated for two hours. Each time point had six replicate wells in the experiment. The absorbance at wavelength of OD 450 nm was measured using a microplate reader (SpectraMax Gemini EM, Molecular Devices, USA). The cell proliferation rate at each time point was calculated based on the OD value as follows: Proliferation rate = $(OD_n - OD_0)/OD_0 \times 100\%$, where OD_n represents the OD value at each time point and OD_0 refers to the initial OD value after cell seeding in medium alone. This experiment was independently repeated three times in our laboratory.

Cell migration assays

The migration ability of cells was assessed using the Transwell assay (Corning, Tewksbury, Massachusetts, USA). Tumor necrosis factor alpha (TNF-α) (200 ng/mL, Cat. #ab183218; Abcam, Cambridge Science Park, UK) was co-cultured with the cells to evaluate their anti-inflammatory potential. The experiment consisted of a TNF-α positive group (TNF-α^+), a TNF-α negative group (TNF-α^-) and a blank control group (cell-free). The Transwell chamber was coated with basement membrane extracts (Cat. #E1270, Sigma-Aldrich, St. Louis, Missouri, USA) for 45 min and then covered at the bottom. A volume of 500 μL medium was added to the lower chamber while the prepared cell suspension (2×10^4 cells) was inoculated into the upper chamber along with 200 μL medium containing or lacking TNF-α. Incubation took place at 37 ℃ in a 5% CO_2 incubator for a migration time of 16–18 h. At the end of this period, the chamber was removed and transferred to a cell superstatic table, where the culture medium was aspirated using a pipette. The membrane was then cleaned using a sterile cotton swab and transferred into a new sterile 24-well plate, to which 500 μL of 4% paraformaldehyde was added to each well. The chamber was held at a 45-degree angle for 10 min to allow cell fixation. Subsequently, the paraformaldehyde solution was discarded, and the cells were rinsed 2–3 times with PBS, and gently dried with a cotton swab. DAPI (1:20) staining in each well was performed for 10 min in the dark. The cells were observed and photographed using an inverted microscope (each well was divided into 15–20 fields of view). The migrated cells were quantified using the ImageJ software. Cell migration rate $(V_1\%)=N_1 / N_2\times100\%$, Migration inhibition rate $(V_2\%) = (N_2-N_3)/N_1\times100\%$, where N_1 represents the initial number of inoculated cells, N_2 represents the number of cells migrated in TNF-α^-, and N_3 represents the number of cells migrated in TNF-α^+. The experiment was independently repeated three times.

Statistical analysis

The experimental data in this study were analyzed using SPSS 26.0 and GraphPad Prism version 8 software (GraphPad Software, San Diego, California USA, www.graphpad.com). Statistical significance was determined at a p-value of less than 0.05. The statistical analysis involved the use of independent sample t-test or two-way analysis of variance. All experimental data are presented as mean ± standard deviation.

Results

CSCs subsets in the three tumor tissues

Single-cell suspensions of appendiceal tumors, peritoneal tumors, and mucosal tissues from six patients were prepared for scRNA-seq analysis. Eleven distinct cell populations were identified by defining the cell subsets, as shown in Table S3 and Fig. 2. These cell populations include epithelial cells, endothelial cells, fibroblasts, smooth muscle cells, cancer stem cells, adipocytes, T cells, B cells, NK cells, macrophages, and granulocytes. Notably, all three tumor tissue types harbored CSCs subsets in varying proportions. Appendiceal tumor tissues exhibited the highest proportion of CSCs (7.64 ± 0.43%), followed by peritoneal tumor tissues (5.71 ± 0.55%), while mucinous tissues displayed the lowest content (3.91 ± 0.13%).

CSCs sorting

The CSCs were obtained by cell sorting. The FlowSight imaging flow cytometer was utilized to detect the presence of $CD133^+$ (R2 gate: 9.98 ± 1.72%), $CD166^+$ (R2 gate: 11.23 ± 1.32%), and $CD133^+/CD166^+$ (R2 gate: 5.6 ± 1.06%) in the mixed cells prior to cell sorting (Fig. 3A). The MACSQuant Tyto system was used to sort $CD133^+$, $CD166^+$, and $CD133^+/CD166^+$ CSCs from the three tissue types. As the mixed cells passed through the microchip laser-sorting device at the bottom of the cartridge, the fluorescently labeled CSCs were sorted into the positive cell compartment, whereas the remaining cells were directed to the negative cell compartment

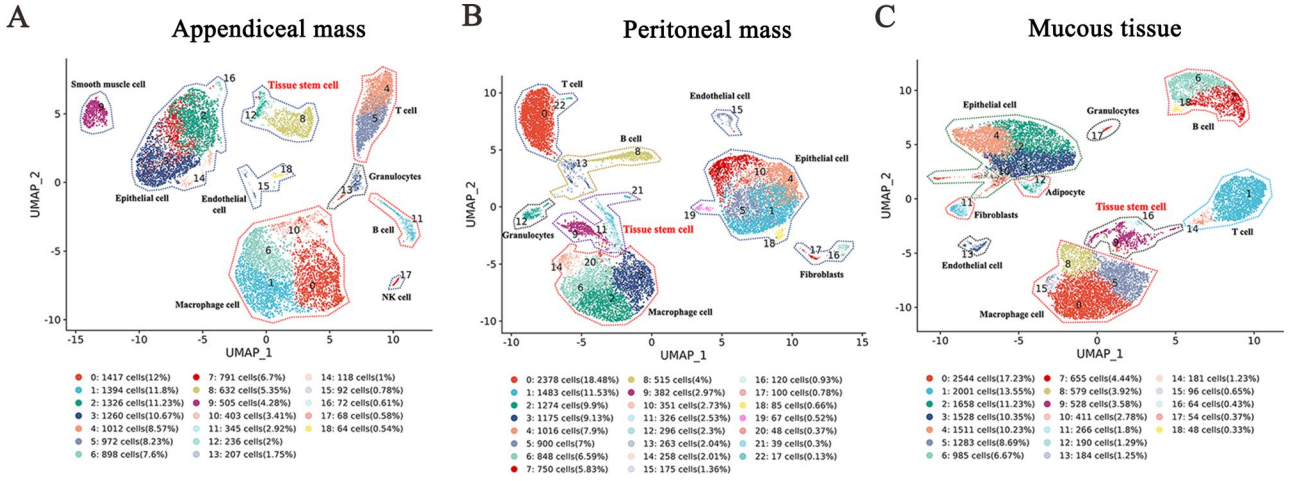

Fig. 2 Cellular composition and content in various tumor tissues. **A**. UMAP visualization of nine distinct cell types in appendiceal tumor tissue. **B**. UMAP visualization illustrating eight different cell types in peritoneal tumor tissue. **C**. UMAP visualization of nine specific cell types in mucinous tumor tissue. Each dot on the UMAP diagram represents an individual cell, with cells of the same type represented by dots of the same color

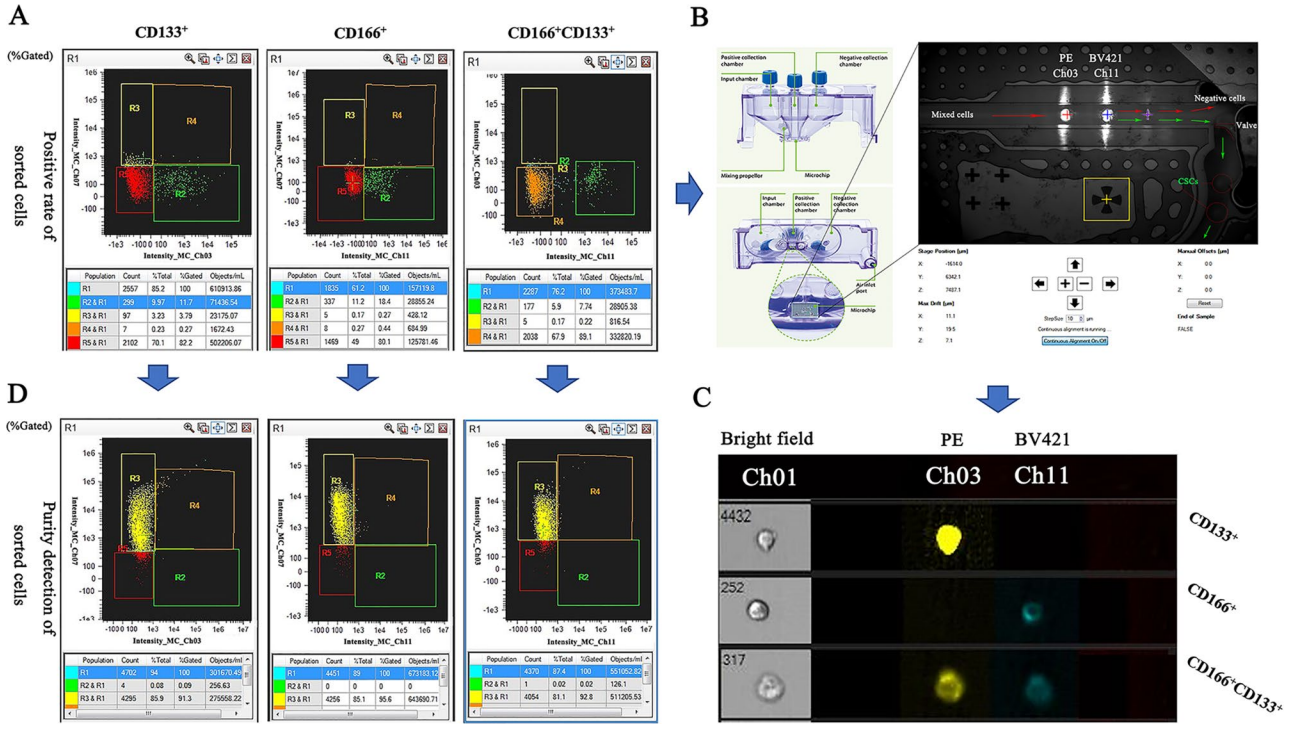

Fig. 3 CSCs sorting process. **A**. Flow cytometry was used to detect $CD133^+$, $CD166^+$, and $CD133^+/CD166^+$ CSCs populations within mixed cells, with the R2 gate serving as the target cell population. **B**. Sorting of CSCs from three tissue classes using the cartridge of the MACSQuant Tyto system, with the cartridge and microchip on the left and cell sorting through the microchip on the right. **C**. Real-time visualization of CSCs obtained by FlowSight imaging flow cytometer. Bright field and cell fluorescence image are presented, with Ch01: light field, Ch03: CD133-PE, and Ch11: CD166-BV421; scale bar = 20 μm. Flow cytometric analysis was performed on the sorted negative cells

(Fig. 3B). Real-time and visual observation of sorted CSCs was conducted using a FlowSight imaging flow cytometer, which enabled the visualization of single-cell membrane expression of both $CD133^+$ and $CD166^+$. Cell viability exceeded 98% (Fig. 3C). Flow cytometry analysis of sorted negative cells revealed a nearly complete absence of $CD133^+$ (R2 gate: 2.27±0.76%), $CD166^+$ (R2 gate: 1.31±0.59%), and $CD133^+/CD166^+$ (R2 gate: 1 0.46±0 0.71%) CSCs (Fig. 3D).

Cell culture and marker identification

The sorted CSCs were seeded in a homemade culture medium and cultured at 37 °C in a humidified incubator with 5% CO_2 (Text S1). Only cells in the logarithmic

growth phase cultured until the third passage were selected. Microscopic examination revealed that all three CSCs types exhibited robust adherence to the cell wall and displayed predominantly fusiform or oval shapes (Fig. 4A). Immunofluorescence staining and flow cytometry were used to identify the expression of $CD133^+$, $CD166^+$, and $CD133^+/CD166^+$ in CSCs (Fig. 4B, C). ImageJ software was used to calculate the positivity rates of the markers from immunofluorescence staining images (Table S4). The results revealed that $CD133^+$ and $CD166^+$ cells had positivity rates ranging from 70 to 80% across all cell types, whereas the positivity rate for $CD133^+/CD166^+$ cells was approximately 30%.

Comparison of cell proliferation, migration, and anti-inflammatory phenotype function

Cell proliferation was assessed using the CCK-8 assay, which revealed that MC had a stronger proliferative ability than PC and AC ($p=0.0212$). However, there was no significant difference in the proliferative abilities of PC and AC cells ($p=0.4403$) (Fig. 5A). To evaluate cell migration and anti-inflammatory ability, cells were co-cultured with TNF-α and the Transwell assay was performed. The number of migrating cells was determined by DAPI staining of nuclei (Fig. 5D). Under normal conditions, the migration rates for MC, AC, and PC were 11.29±2.38%, 10.27±0.79%, and 12.02±1.07% respectively; whereas in an inflammatory environment induced by TNF-α treatment, the migration rates were 9.74±1.29% for MC, 2.74±0.64% for AC, and 7.73±0.42% for PC (Fig. 5B, Table S5). The inhibition rates from TNF-α on cell migration were 18.09±0.09% for MC, 73.07±0.13%, for AC, and 35.04±0.16% for PC (Fig. 5C). Statistical analysis showed no significant difference in CSCs' migration ability among the three types under normal conditions ($p=0.1802$), while TNF-α exerted the greatest inhibitory effect on the migration ability of AC ($p<0.0001$).

Discussion

Currently, there are few studies focusing on CSCs in PMP. This may be attributed to the rarity of PMP, and the difficulties with early diagnosis. By the time the disease is diagnosed, patients often have already undergone multiple abdominal organ surgeries, including the removal of primary lesions such as those in the appendix, resulting in a scarcity of samples for research [22]. Additionally, owing to their limited presence within the tumor cell population, defining and isolating CSCs with high purity and viability poses significant difficulties.

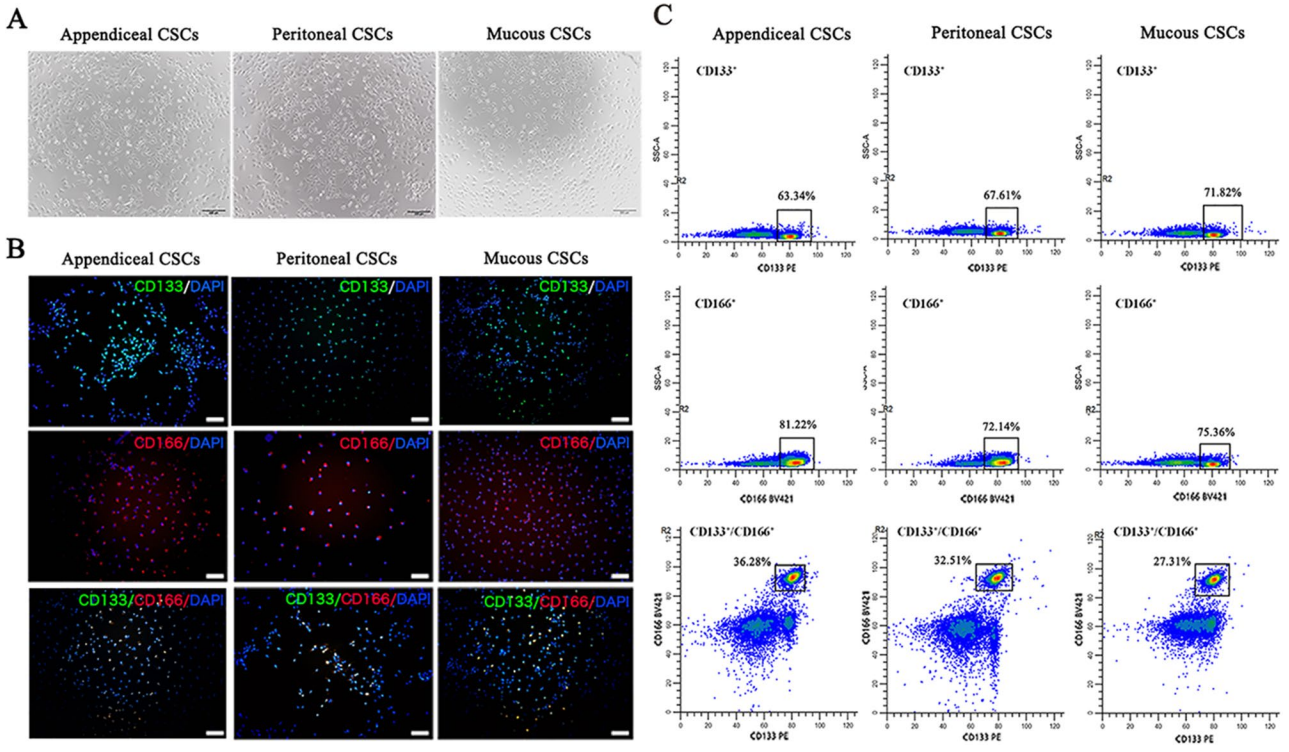

Fig. 4 Cell culture and marker identification. **A**. Observation of cell growth using a light microscope revealed the morphology, size, and adherence of cells in the logarithmic growth phase, with a scale bar indicating 100 μm. **B**. Immunofluorescence staining was performed to detect markers. Nuclei are stained blue, $CD133^+$ appears as green fluorescence, $CD166^+$ appears as red fluorescence, and $CD133^+/CD166^+$ appears as yellow fluorescence. Scale bar indicates 200 μm. **C**. Marker detection was also conducted using flow cytometry, where each colored point represents a cell. The target cell population is enclosed by a black box for clarity, with brighter colors indicating a higher cell density

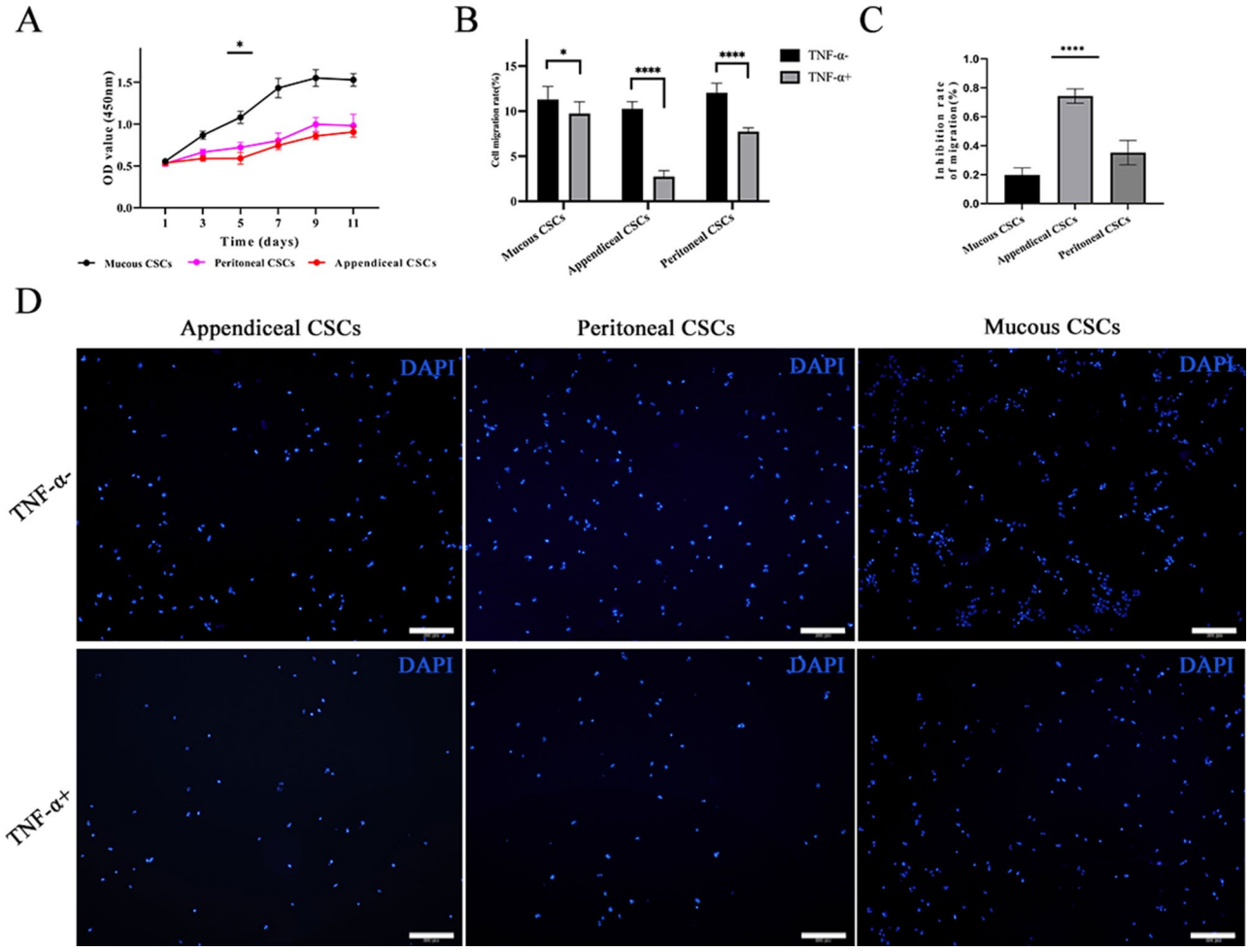

Fig. 5 Comparative analysis of cellular proliferation, migration, and anti-inflammatory phenotypes **A**. Cell proliferation was assessed using the CCK-8 assay with cells cultured for 1, 3, 5, 7, 9, and 11 days. **B** and **C**. Co-culturing cells with TNF-α enabled evaluation of cell migration and anti-inflammatory potential through Transwell assays. The bar graph illustrates the rates of cell migration and inhibition of migration. Error bars represent standard error of the mean. **D**. Cell migration was visualized by nuclear staining using DAPI; the scale bar represents 200 μm

This study represents a pioneering effort to elucidate the presence of a distinct subpopulation of CSCs within PMP at the single-cell level. Appendiceal, peritoneal, and mucinous tumor tissues harbored varying proportions of CSCs subsets, with the appendiceal tumor tissue exhibiting the highest abundance and the mucinous tissue displaying the lowest. Furthermore, diverse cell types, such as macrophages and T cells, were prominent in tumor tissues. Therefore, investigation of the immune microenvironment surrounding these neoplastic cells is imperative for future research.

Based on the sequencing results, the CSCs were successfully sorted using MACSQuant Tyto and FlowSight imaging flow cytometers [23]. The MACSQuant Tyto is a hermetically sealed sterile sorting system. The sorting process takes place within a sealed cartridge designed in the shape of a "boat," allowing for reduction of sorting pressure to 2 kPa. Moreover, owing to the absence of sheath fluids and fluid tubes within the sorting chamber, the cells are not subjected to shear forces, decompression, or charging. Most importantly, cells can undergo multiple consecutive sorting without compromising viability, resulting in enhanced purity and viability of target cells [24]. The sorted CSCs were passaged stably until the fifth generation. Morphological observations showed that the cells were plow-shaped, and most were fusiform or oval. Immunofluorescence staining and flow cytometry were used to determine the expression of CD133, CD166, and CD133/CD166 in the CSCs. The results demonstrated the stable expression of these markers in CSCs with a purity of up to 80%. These findings not only laid a foundation for subsequent cell experiments but also validated the reliability of this novel cell sorting method.

Cell proliferation, migration, and anti-inflammatory properties play crucial roles in tumor recurrence and metastasis. The inhibitory effect of TNF-α on both cell proliferation and migration has been observed [25]. In this study, we investigated the proliferation, migration,

and anti-inflammatory capacities of the three types of CSCs. The findings revealed that MC exhibited the highest proliferation and anti-inflammatory capacity, whereas AC displayed the weakest proliferation ability. TNF-α exerted the strongest inhibitory effect on AC cell migration.

A prominent characteristic of patients with PMP is the extensive dissemination of gelatinous mucus within the peritoneal cavity. The present study suggests that MC populations demonstrate superior proliferative and anti-inflammatory capabilities. Hence, it can be inferred that the presence of highly proliferative and anti-inflammatory MC contributes to the challenge of surgical mucus removal, and renders these cells resistant to chemotherapy. The proliferation and anti-inflammatory abilities of AC, however, are limited, suggesting that AC are early or immature CSCs.

These results indicate that these CSCs possess distinct characteristics and are not identical; AC are more inert, whereas MC and PC in the peritoneal cavity are more active. Clinical evidence has demonstrated that the tumor tissue within the appendix can remain dormant in its lumen for up to 10–20 years [26]. However, once it invades the serosal layer (without visible rupture), rapid implantation and metastasis occur within the abdominal cavity, thereby accelerating disease progression [27]. Therefore, considering the clinical manifestations, it is plausible to suggest that the differences in cellular function may be attributed to variations in the abdominal microenvironment. Consequently, future research focusing on understanding the tumor microenvironment within the abdominal cavities of patients with PMP is required.

Conclusions

MC, AC, and PC were successfully isolated from patients with PMP using MACSQuant tyto sorting and FlowSight imaging flow cytometry, followed by subculturing and identification. Comparison of cell function revealed that the appendiceal tumor tissue had a high CSCs content which exhibited an indolent nature and weak anti-inflammatory ability. Although the content of CSCs in mucous tissue was low, the cells in MC have strong proliferation, migration and anti-inflammatory abilities. Overall, this study provides preliminary insights into the biological characteristics of CSCs in different cancer foci and offers reference data for future targeted CSCs therapies. In addition, this study presents a novel cell-sorting strategy. Furthermore, when combined with the clinical manifestations, we hypothesized that the functional differences among these three classes of CSCs may be attributed to variations in the microenvironment at their respective implantation sites within the abdominal cavity. Early detection of malignant changes in the appendix and prompt resection interventions are crucial to prevent disease progression and metastasis.

Abbreviations

AC	Appendiceal cancer stem cells
CRS	Cytoreductive surgery
CSCs	Cancer stem cells
HIPC	Hyperthermic intraperitoneal chemotherapy
MC	Mucous cancer stem cells
PC	Peritoneal cancer stem cells
PMP	Pseudomyxoma peritonei
scRNA-seq	Single-cell mRNA sequencing

Supplementary Information

The online version contains supplementary material available at https://doi.org/10.1186/s12967-024-05730-6.

Supplementary Material 1

Supplementary Material 2

Supplementary Material 3

Supplementary Material 4

Supplementary Material 5

Supplementary Material 6

Acknowledgements

The authors appreciate the technical support and other help from Qihong Chen, Tan Min, Changhai QI, Shi Han, Jingxuan Jiao, Xiaozhi Sun and Huan Gou. We would like to thank Editage (www.editage.cn) for English language editing.

Author contributions

HPZ, HBX, and RQM designed the experiments. HPZ, SJP, LBA, GJS, CW, PZ, XWF, LFY, FC and RQM performed tissue acquisition. HPZ, HBX and RQM analysed the data. JY and SYT contributed materials/reagents/analysis tools. YYL provided pathology consultation. HPZ wrote the manuscript.

Funding

This research was supported by the Sponsored by Science Foundation of AMHT (NO. 2023YK06), Research Fund of Aerospace Center Hospital (YN202410 and YN202424) and the Beijing Gold-Bridge Project (No. ZZ21043).

Data availability

The datasets used and/or analysed during the current study are available from the corresponding author on reasonable request.

Declarations

Ethics approval and consent to participate

All human tissues were handled in accordance with protocols approved by the hospital's Ethics Committee (Application No. 2024-024). The patients or their guardians/legally authorized representatives/next of kin provided written informed consent for the use of samples.

Consent for publication

Not applicable.

Competing interests

The authors have no conflicts of interest to declare.

Received: 17 March 2024 / Accepted: 6 October 2024
Published online: 14 November 2024

References

1. Sugarbaker PH. Pseudomyxoma Peritonei. Cancer Treat Res. 1996;81:105–19.
2. Spyropoulos C, Rentis A, Alexaki E, Triantafillidis JK, Vagianos C. Appendiceal mucocele and pseudomyxoma peritonei; the clinical boundaries of a subtle disease. Am J Case Rep. 2014;15:355–60.
3. Wang B, Yao J, Ma R, Liu D, Lu Y, Shi G, An L, Xia A, Chen F, Pang S, Zhai X, Liu G, Chen S, Xu M, Song L, Xu H. The mutational landscape and prognostic indicators of pseudomyxoma peritonei originating from the ovary. Int J Cancer. 2021;148(8):2036–47.
4. Govaerts K, Lurvink RJ, De Hingh IHJT, Van der Speeten K, Villeneuve L, Kusamura S, Kepenekian V, Deraco M, Glehen O, Moran BJ, PSOGI. Appendiceal tumours and pseudomyxoma peritonei: literature review with PSOGI/EURACAN clinical practice guidelines for diagnosis and treatment. Eur J Surg Oncol. 2021;47(1):11–35.
5. Hinson FL, Ambrose NS. Pseudomyxoma Peritonei. Br J Surg. 1998;85(10):1332–9.
6. Smeenk RM, Bruin SC, van Velthuysen ML, Verwaal VJ. Pseudomyxoma Peritonei. Curr Probl Surg. 2008;45(8):527–75.
7. Mittal R, Chandramohan A, Moran B. Pseudomyxoma peritonei: natural history and treatment. Int J Hyperth. 2017;33(5):511–9.
8. Narasimhan V, Wilson K, Britto M, Warrier S, Lynch AC, Michael M, Tie J, Akhurst T, Mitchell C, Ramsay R, Heriot A. Outcomes following cytoreduction and HIPEC for Pseudomyxoma Peritonei: 10-Year experience. J Gastrointest Surg. 2020;24(4):899–906.
9. Ma R, Lu D, Xue S, Fan X, Zhai X, Wang C, Xu H, Pang S. Preoperative systemic chemotherapy does not benefit for appendiceal pseudomyxoma peritonei. ANZ J Surg. 2023;93(1–2):219–26.
10. Gholamzad A, Khakpour N, Khosroshahi EM, Asadi S, Koohpar ZK, Matinahmadi A, Jebali A, Rashidi M, Hashemi M, Sadi FH, Gholamzad M. Cancer stem cells: the important role of CD markers, signaling pathways, and MicroRNAs. Pathol Res Pract. 2024;256:155227.
11. Prince ME, Sivanandan R, Kaczorowski A, Wolf GT, Kaplan MJ, Dalerba P, Weissman IL, Clarke MF, Ailles LE. Identification of a subpopulation of cells with cancer stem cell properties in head and neck squamous cell carcinoma. Proc Natl Acad Sci U S A. 2007;104(3):973–8.
12. Singh SK, Clarke ID, Hide T, Dirks PB. Cancer stem cells in nervous system tumors. Oncogene. 2004;23(43):7267–73.
13. Al-Hajj M, Wicha MS, Benito-Hernandez A, Morrison SJ, Clarke MF. Prospective identification of tumorigenic breast cancer cells. Proc Natl Acad Sci U S A. 2003;100(7):3983–8.
14. Li C, Lee CJ, Simeone DM. Identification of human pancreatic cancer stem cells. Methods Mol Biol. 2009;568:161–73.
15. Sainz B Jr, Heeschen C. Standing out from the crowd: cancer stem cells in hepatocellular carcinoma. Cancer Cell. 2013;23(4):431–3.
16. Barzegar Behrooz A, Syahir A, Ahmad S. CD133: beyond a cancer stem cell biomarker. J Drug Target. 2019;27(3):257–69.
17. Ferragut F, Vachetta VS, Troncoso MF, Rabinovich GA, Elola MT. ALCAM/CD166: a pleiotropic mediator of cell adhesion, stemness and cancer progression. Cytokine Growth Factor Rev. 2021;61:27–37.
18. Hermann PC, Trabulo SM, Sainz B Jr, Balic A, Garcia E, Hahn SA, Vandana M, Sahoo SK, Tunici P, Bakker A, Hidalgo M, Heeschen C. Multimodal Treatment eliminates Cancer Stem cells and leads to long-term survival in primary human pancreatic Cancer tissue xenografts. PLoS ONE. 2013;8(6):e66371.
19. Abbas G, Saluja TS, Kumar D, Agrawal H, Gupta A, Panday G, Singh SK. Antitumor efficacy of synthesized Ag-Au nanocomposite loaded with PEG and ascorbic acid in human lung cancer stem cells. Exp Cell Res. 2024;435(1):113904.
20. Kim H, Jang B, Zhang C, Caldwell B, Park DJ, Kong SH, Lee HJ, Yang HK, Goldenring JR, Choi E. Targeting stem cells and dysplastic features with Dual MEK/ERK and STAT3 suppression in gastric carcinogenesis. Gastroenterology. 2024;166(1):117–31.
21. Moradi L, Tajik F, Saeednejad Zanjani L, Panahi M, Gheytanchi E, Biabanaki ZS, Kazemi-Sefat GE, Hashemi F, Dehghan Manshadi M, Madjd Z. Clinical significance of CD166 and HER-2 in different types of gastric cancer. Clin Transl Oncol. 2024;26(3):664–81.
22. Sugarbaker PH. New standard of care for appendiceal epithelial neoplasms and pseudomyxoma peritonei syndrome? Lancet Oncol. 2006;7(1):69–76.
23. Verma JR, Harte DSG, Shah UK, Summers H, Thornton CA, Doak SH, Jenkins GJS, Rees P, Wills JW, Johnson GE. Investigating FlowSight® imaging flow cytometry as a platform to assess chemically induced micronuclei using human lymphoblastoid cells in vitro. Mutagenesis. 2018;33(4):283–9.
24. Zhou H, He Y, Wang Z, Wang Q, Hu C, Wang X, Lu S, Li K, Yang Y, Luan Z. Identifying the functions of two biomarkers in human oligodendrocyte progenitor cell development. J Transl Med. 2021;19(1):188.
25. Huyghe J, Priem D, Bertrand MJM. Cell death checkpoints in the TNF pathway. Trends Immunol. 2023;44(8):628–43.
26. Sugarbaker PH. Peritoneal metastases, a Frontier for Progress. Surg Oncol Clin N Am. 2018;27(3):413–24.
27. Carr NJ, Cecil TD, Mohamed F, Sobin LH, Sugarbaker PH, González-Moreno S, Taflampas P, Chapman S, Moran BJ, Peritoneal Surface Oncology Group International. A Consensus for classification and Pathologic Reporting of Pseudomyxoma Peritonei and Associated Appendiceal Neoplasia: the results of the Peritoneal Surface Oncology Group International (PSOGI) modified Delphi process. Am J Surg Pathol. 2016;40(1):14–26.

Publisher's note